Research Square

Preprints are preliminary reports that have not undergone peer review.
They should not be considered conclusive, used to inform clinical practice,
or referenced by the media as validated information.

Integrated longitudinal metabolome and proteome analysis provides new insights into metabolic dysregulations in amyotrophic lateral sclerosis

Xiaojiao Xu
University of Electronic Science and Technology of China
Zheyi Liu
Chinese Academy of Sciences Dalian Institute of Chemical Physics
Qiu Yang
University of Electronic Science and Technology of China
Rong Zhang
Sichuan Provincial People's Hospital: Sichuan Academy of Medical Sciences and Sichuan People's Hospital
Hang Yu
Sichuan Provincial People's Hospital: Sichuan Academy of Medical Sciences and Sichuan People's Hospital
Manli Wang
University of Electronic Science and Technology of China
Sheng Chen
Shanghai Jiao Tong University Medical School Affiliated Ruijin Hospital
Guowang Xu
Chinese Academy of Sciences Dalian Institute of Chemical Physics
Yaping Shao
First Affiliated Hospital of Dalian Medical University
Weidong Le (wdle_sibs@163.com)
Sichuan Provincial People's Hospital: Sichuan Academy of Medical Sciences and Sichuan People's Hospital https://orcid.org/0000-0001-7459-2705

Research Article

Keywords: ALS, metabolomics, proteomics, LC-MS, Purine metabolism, energy metabolism

Posted Date: September 20th, 2022

DOI: https://doi.org/10.21203/rs.3.rs-2040018/v1

License: This work is licensed under a Creative Commons Attribution 4.0 International License. Read Full License

Abstract

Background

Amyotrophic lateral sclerosis (ALS) is an irreversible fatal neurodegenerative disease with progressive paralysis of limbs and bulb in patients, the cause of which remains unclear. Due to the highly heterogeneous and complex pathophysiology of the disease, there is currently no effective treatment to retard the disease progression. Accumulating studies suggest that motor neuron degeneration is associated with systemic metabolic impairment in ALS. However, the metabolic reprogramming and underlying mechanism in the longitudinal progression of the disease remain poorly understood.

Methods

Here, we applied unbiased LC-MS-based metabolomics to plasma, lumbar spinal cord, and motor cortex tissues from SOD1^{G93A} mice and wildtype (WT) littermates at different stages to explore the metabolic disturbance during disease progression. To elucidate the regulatory network underlying metabolic changes, spinal cords from SOD1^{G93A} and WT mice in the symptomatic stage were further analyzed by proteomics.

Results

The results show that SOD1^{G93A} mice presented marked dysregulations of lipid and purine metabolism in both plasma and spinal cord from the pre-symptomatic stage. Furthermore, the metabolic abnormalities were much more pronounced in the symptomatic stage. By integrating metabolomics and proteomics data, we demonstrated the importance of metabolic pathways in the tricarboxylic acid (TCA) cycle, arginine and proline metabolism, and fatty acid degradation in the progression of ALS pathophysiology.

Conclusions

Notably, for the first time, we highlighted that metabolic dysregulation in purine metabolism might be a critical event in the preclinical phase of ALS. The identified differential metabolites and proteins in our study complement existing data on metabolic reprogramming in ALS; the results from the integrative analysis might provide novel perspectives for early diagnosis and therapeutic intervention of the disease.

Background

Amyotrophic lateral sclerosis (ALS) is a lethal neurodegenerative disease, characterized by progressive loss of upper and lower motor neurons [1–2]. The clinical presentation of ALS typically begins with weakness in one focused area and then spreads to multiple sites, including the bulbar, limb, and thoracic muscles. Patients with ALS eventually die of respiratory failure after 2–5 years of evolution [3]. Due to the difference in the involvement of upper and lower motor neurons, ALS patients usually present with different initial symptoms. The lack of effective biomarkers further makes it difficult for clinicians to make a definitive diagnosis and provide timely interventions in the early stages of the disease [2–3].

It has been hypothesized that genetic mutations, glutamate excitotoxicity, neuroinflammation, protein misfolding, oxidative stress, and mitochondrial dysfunction are implicated in the pathogenesis of ALS [2, 4]. However, the precise etiology and pathogenesis remain unknown. Omics technologies such as metabolomics and proteomics have been widely used in recent decades as powerful tools for the discovery of novel biomarkers, identification of therapeutic targets, and elucidation of the pathogenesis of diseases [5]. Many recent studies have found that metabolic abnormalities, particularly defective energy and lipid metabolism, play important roles in the pathophysiology of ALS [6–8]. Previous studies have reported that patients with ALS had a lower body mass index, which was positively associated with ALS risk [9–10]. Reduced triacylglycerol levels were documented in the plasma and cerebrospinal fluid of ALS patients, and elevated triglyceride level was found to be highly correlated with prolonged survival [11–12]. Abnormalities in glucose utilization and adenosine 5'-triphosphate (ATP) generation have been reported in the brain and spinal cords of both ALS patients and ALS mice models, which may result in the impairment of mitochondria and motor neurons [13–14]. Sphingomyelins, ceramides, fatty acid metabolism, and branched amino acid metabolism have also been found to be disrupted in ALS [15–18].

Nevertheless, the underlying mechanisms of the metabolic dysregulation in ALS remain unclear, and it may be the result of complex biochemical regulation at multiple levels. The synthesis and degradation of metabolites are intricately linked to the catalyzation of enzymes and the regulation of signaling pathways. Changes in the enzymes involved in energy metabolism in ALS were reported by a targeted proteomic study [19]. Combined metabolomics and proteomics analysis may help to uncover the underlying biological relationships and improve understanding of the entire metabolic network regulation and has been widely used to investigate neurodegenerative diseases recently [20]. The combination of metabolomics and proteomics would aid in the identification of key metabolic drivers in disease development and could also assist in the understanding of the interaction between disturbed metabolic pathways and pathophysiological changes [21–22]. However, there are few integrative studies on ALS. Furthermore, many ALS studies are case-control studies that focused on molecular alterations in biofluids or tissues from patients or animal models, and studies of longitudinal progression that monitored disease at multiple time points are rare.

$SOD1^{G93A}$ transgenic mice have been widely used as a model of ALS in preclinical studies, and they recapitulate the main symptoms of ALS, including motor neuron degeneration and muscle denervation, eventually causing progressive paralysis and death [23]. In this study, we collected plasma, motor cortex, and lumbar spinal cord from $SOD1^{G93A}$ mice and age-matched littermates at different stages for liquid chromatography-mass spectrometry (LC-MS)-based untargeted metabolomic analysis. By investigating the metabolic differences between $SOD1^{G93A}$ mice and wildtype (WT) mice using biostatistical and bioinformatic approaches, we aimed to uncover the metabolic signature associated with disease progression in various biological samples. Furthermore, for the first time, we performed an integrative analysis of metabolomics and proteomics in the lumbar spinal cords of symptomatic $SOD1^{G93A}$ mice and their littermates. We attempted to identify the most critical metabolic pathways involved in ALS pathophysiological changes and elucidate the regulation mechanism underlying the metabolic changes, which might provide new insights into ALS pathogenic mechanisms.

Methods And Materials

Animals and sample collection

Transgenic $SOD1^{G93A}$ mice were originally purchased from Jackson Laboratory (B6SJL-Tg (SOD1*G93A) 1Gur/J, 002726). Breeding was maintained by crossing $SOD1^{G93A}$ hemizygous males with WT B6SJL females. Polymerase chain reaction (PCR) was used for genotyping, as reported previously [24]. The mice were housed in a pathogen-free room with a controlled temperature and humidity facility (12/12 h light/dark, lights on at 7:00 a.m.), and fed with sterilized granular rodent food and sterile water. Because the spinal cord and motor cortex are two common lesion sites involved in ALS, we collected the lumbar spinal cord, motor cortex, and blood from male and female $SOD1^{G93A}$ mice at 60 days (the pre-symptomatic stage) and 120 days of age (the symptomatic stage) for metabolomics analysis. Age-matched WT littermates served as controls (**Figure S1, Tables S1, and S2**). Blood samples were taken from the inner canthus with a glass capillary. Plasma was isolated using ethylene diamine tetraacetic acid as an anticoagulant. At each time point, the $SOD1^{G93A}$ mice and their littermates were sacrificed, and the lumbar spinal cord and motor cortex were separated. All tissues and plasma samples were immediately stored at − 80 °C until further analysis. All experiments were carried out following the guidelines of the Institutional Animal Care and Use Committee. All procedures for animal experiments were approved by Dalian Medical University's Ethics Committee.

Sample preparation for metabolomics analysis

Plasma samples were thawed on ice and pretreated according to our previous protocol [25–26]. Briefly, 60 μL of plasma was deproteinized by adding 240 μL of methanol containing 14 internal standards (ISs, **Table S3**). The mixture was vortexed and centrifuged for 15 min (13,000 *g*, 4°C). Then, the supernatant was divided into two aliquots and dried in a vacuum centrifugal concentrator (CentriVap, Labconco, USA). Before LC-MS analysis, the dried powder was reconstituted with 60 μL of 25% (v/v) aqueous methanol. Additionally, QC samples were made by mixing 10 μL of each plasma sample and prepared as described above. Frozen lumbar spinal cord and motor cortex tissues (about 10 mg) were spiled with 1 mL methanol containing 11 ISs (**Table S4**). The mixture was homogenized using a mixer mill (MM400, Retsch Technology, Germany), followed by centrifugation (13,000 *g*, 15 min, 4°C). The supernatant was divided into two aliquots and freeze-dried. The dried sample was reconstituted with 60 μL of 50% (v/v) aqueous methanol. QC samples were prepared by pooling an equal volume of metabolite extracts from every tissue sample.

Sample preparation for proteomics analysis

The mouse spinal cords were lysed with a homogenizer and the proteins were extracted by precipitation. The protein pellets were resuspended in digestion buffer (8 M Urea 50 mM NH_4HCO_3 pH 8.0) and the protein concentration was determined by BCA assay. The proteins were first reduced by Tris (2-carboxyethyl) phosphine to open the disulfide linkages, followed by alkylation with Iodoacetamide to block the thiols of cysteine. The proteins were then digested by Lys-C at 37°C for 1 h with a ratio of 1:100 (enzyme: protein, w/w), and then the concentration of urea was diluted to 1 M by adding 50 mM NH_4HCO_3 (pH 8.0). The proteins were further digested by adding trypsin with a ratio of 1:50 (enzyme: protein, w/w) at 37°C overnight. The digestion was quenched by acidification and the samples were desalted by SPE columns.

Non-targeted LC-MS-based metabolomics analysis

LC-MS differentiation and detection of each metabolite were performed using Ultra-Performance Liquid Chromatography (Waters Corporation, Manchester, UK) coupled with the Triple TOF™ 5600 PLUS (Applied Biosystems, Foster City, CA) mass spectrometry system. In positive ion mode, an ACQUITY UPLC BEH C8 column (1.7 μm, 2.1 mm × 100 mm) was used for chromatographic separation. The mobile phases were 0.1% formic acid aqueous solution and 0.1% formic acid acetonitrile. In negative ion mode, an ACQUITY UPLC HSS T3 column (1.8 μm, 2.1 mm × 100 mm) was used. The mobile phases were water and 95% methanol (v/v) (both containing 6.5 mM NH4HCO3). The injection volume was 5 μL, and the column temperature was set to 50 °C. The gradient elution profile and mass spectrometry parameters were set as previously described [25, 27]. In addition, IDA-based auto-MS^2 was performed on the 15 most intense metabolite ions in a cycle of the full scan to acquire qualitative information for metabolite identification. Data acquisition and instrument control were conducted using Analyst TF 1.7 software.

LC-MS/MS-based proteomics analysis

The protein digests were resuspended in Buffer A (0.1% formic acid in H_2O) and analyzed by LC-MS/MS. All the proteomic data were collected by Thermo Fusion Lumos mass spectrometry coupled with the Vanquish Flex HPLC system (ThermoFisher Scientific). About 1 μg protein digest was first loaded onto a 5 cm × 150 μm C18 trap column (5 μm C18, SunChrom) with a flow rate of 5 μL/min. The peptides were separated by a 15 cm × 150 μm

C18 capillary column (2.4 μm C18, Dr. Maisch) at a flow rate of 0.3 μL/min. The elution gradient was set from 5–32% Buffer B (0.1% formic acid in acetonitrile) in 60 min. The eluted peptides were introduced into MS by electrospray ionization with a spray voltage of 2 kV. The MS was working in positive mode. The MS1 spectra were collected by Orbitrap analyzer with a resolution of 120 K and a scan range of 300–1650 m/z. The MS2 spectra were also collected in a data-dependent mode and top-speed manner (3 s). The precursor ions with a charge state of 2–5 were isolated by quadrupoles with an isolation width of 1.6 m/z and then subjected to HCD with normalized energy of 30. The fragment ions were collected by Orbitrap analyzer with a resolution of 15,000. Dynamic exclusion was enabled with an exclusion time of 60 s.

Raw data processing

The metabolomics raw data were imported into Marker View software (Version 1.2.1.1, Applied Biosystems) for peak detection and alignment. Metabolites were annotated using an in-house database by comparison of the ion features in QC samples with the reference chemical standards using OSI/SMMS software. [28]. MultiQuant software (version 2.1, Applied Biosystems) was used to integrate chromatographic peaks of the annotated metabolites in tissue samples. The missing values were removed according to the 80% rule [29]. Before statistical analysis, the original peak area of each retained peak was calibrated by ISs. For proteomics, the MS raw data were processed by Maxquant (version 1.6.7). The mouse proteome dataset was downloaded from Uniprot for search. The protease was set as Trypsin with a max miss cleavage of 2. Label-free quantification was enabled. The function of the match between runs was also enabled to increase the analysis depth. The other parameters were set as default values.

Statistical analysis

Multivariate analyses (PCA, PLS-DA, and OPLS-DA) were performed using SIMCA-P 14.1 software (Umetric AB, Umea, Sweden). The student's t-test was used to calculate the statistical difference ($p < 0.05$ is considered statistically significant). Online software MetaboAnalyst (http://www.metaboanalyst.ca) was used for pathway enrichment analysis. Multi Experiment Viewer software (version 4.7.4) was used to construct the heat map. The metabolic pathway was constructed according to the Kyoto Encyclopedia of Genes and Genomes (KEGG) database (https://www.kegg.jp/). The NAguideR tool with the impseq approach (sequential imputation) was used to interpolate the missing values of the proteomics data [30].

Functional enrichment and protein interaction network analysis

Gene ontology (GO) analysis and KEGG pathway analysis were performed using the Database for Annotation, Visualization and Integrated Discovery (DAVID, http://david.abcc.ncifcrf.gov/) and KOBAS 3.0 databases (http://kobas.cbi.pku.edu.cn/kobas3/) online program. The Search Tool for the Retrieval of Interacting Genes (STRING, https://cn.string-db.org/) was used for the protein-protein interaction (PPI) analysis, and the minimum required interaction score was set as 0.4. Cytoscape 3.9.0 software (download from https://cytoscape.org/) was used to visualize the PPI network. Significant modules in the PPI network were screened by the Molecular Complex Detection (MCODE) plugin. The criteria for selection were set as follows: MCODE scores > 3, number of nodes > 5, degree cut-off = 2, node score cut-off = 0.2, k-score = 2, and Max depth = 100. KEGG pathway enrichment analysis was performed for proteins involved in these modules.

Results

Data quality assessment

After raw data processing and structure identification using our in-house metabolite database, 367 specific metabolites in plasma and 304 in tissue samples were identified and used for the following statistical analysis. To evaluate the stability and repeatability of the analytical method, quality control (QC) samples were constructed by pooling equal amounts of extracts from all plasma or tissue samples, and then aliquoted and analyzed every 10 sample runs. Univariate analysis of all annotated metabolites in QC samples showed that 99.73% and 94.08% of all identified metabolites had relative standard deviation (RSD) values less than 30% in plasma and tissues, respectively (**Figure S2A, 2D**). Moreover, the principal component analysis (PCA) scores plot showed that the QC samples clustered tightly, with the majority of samples falling within mean ± 2 SD in the first principal component direction (**Figure S2B-C, E-F**). These results demonstrate that the metabolomic data are reliable and robust.

The metabolic disturbance was more prominent in the symptomatic stage

To investigate the dynamic metabolic changes in the progression of ALS, $SOD1^{G93A}$ mice at 60 and 120 days of age and age-matched WT mice were studied by metabolomic assays. These time points correspond to the pre-symptomatic and symptomatic stages, respectively. At 60 days of age, there were no obvious motor symptoms, and only mild pathological changes were noted in $SOD1^{G93A}$ mice [31]. At 120 days of age, all $SOD1^{G93A}$ mice exhibited obvious motor symptoms and muscle denervation along with pathological changes [31]. Accordingly, the metabolic profiles of 60- and 120-day-old $SOD1^{G93A}$ mice could fully reveal metabolic alterations under different pathological conditions of ALS. As shown in the orthogonal partial least-squares discrimination analysis (OPLS-DA) scores plot, the metabolic signatures of both WT and $SOD1^{G93A}$ mice at the symptomatic stage differed from those at the pre-symptomatic stage. The metabolic discrepancy between WT and $SOD1^{G93A}$ mice was found to be more pronounced at the symptomatic stage (120d) in plasma, spinal cord, and cortex (Fig. 1A–C), suggesting that metabolic alterations in the symptomatic stage were more pronounced and complicated.

When comparing symptomatic SOD1^{G93A} mice with WT mice, 77 differentially expressed metabolites (DEMs) ($p < 0.05$, t-test; variable importance in projection (VIP) > 1) were found in the plasma (Fig. 1D). These DEMs were primarily lipids (about 66%), including the free fatty acid (FFA), phosphatidylcholine (PC), lysophosphatidylcholine (LPC), phosphatidylethanolamine (PE), and phosphatidylethanolamine (LPE) families (Fig. 1E). The rest of the DEMs were mainly amino acids (Fig. 1E). Apart from FFAs, we found that most lipids were reduced in SOD1^{G93A} mice. In addition, amino acids, including lysine, arginine, proline, several amino acid derivatives, and myo-inositol also decreased in SOD1^{G93A} mice (Fig. 1D). To identify the relevant metabolic pathways that contributed to the pathophysiology of ALS, these DEMs were further subjected to pathway enrichment analysis. The results show that the most significantly perturbed pathways in the symptomatic stage were linoleic acid and α-linolenic acid metabolism, cysteine and methionine metabolism, arachidonic acid metabolism, and glycerophospholipid metabolism (Fig. 1F).

In the spinal cord, 47 metabolites ($p < 0.05$, t-test; VIP > 1) were found to be differentially expressed in SOD1^{G93A} mice (Fig. 2A-B). A heat map was generated to better depict the DEMs levels in WT and SOD1^{G93A} mice (Fig. 2C). In contrast with plasma, levels of differential lipids in the spinal cord were elevated, except glycerol 3-phosphate, PC 36:2, and PC 40:6. Meanwhile, intermediate metabolites in glycolysis (glucose 6-phosphate and fructose-1,6-bisphosphate) and cis-aconitic acid were found to be increased in SOD1^{G93A} mice (Fig. 2C). Notably, we found a global reduction in purines and purine derivatives (adenine, adenosine 5′-monophosphate (AMP), guanosine 5′-diphosphate (GDP), guanosine 3′,5′-cyclic monophosphate (cGMP), 2′-Deoxyguanosine 5′-monophosphate (dGMP), and allantoic acid) in SOD1^{G93A} mice (Fig. 2C). The pathway analysis also revealed that purine metabolism, glycerophospholipid metabolism, and sphingolipid metabolism were the most significantly disturbed pathways in the spinal cord of SOD1^{G93A} mice during the symptomatic stage (Fig. 2D).

In contrast with spinal cord, only 28 DEMs were screened in the motor cortex during the symptomatic stage ($p < 0.05$, t-test; VIP > 1, **Figure S3A–C**). These DEMs were mainly involved in arachidonic acid metabolism, glutathione metabolism, starch and sucrose metabolism, and inositol phosphate metabolism, among others (**Figure S3D**).

Metabolic disturbance in the pre-symptomatic stage

Since pre-symptomatic ALS is the best time for early intervention and treatment of the disease, we investigated whether pre-symptomatic ALS had distinct metabolic profiles. Although the metabolic alterations in the pre-symptomatic stage (60d) were less prominent than those in the symptomatic stage (120d), the partial least-squares discrimination analysis (PLS-DA) scores plot showed that there was still clear discrimination in the metabolic profile of plasma between WT and SOD1^{G93A} mice (Fig. 3A). In total, 23 DEMs were screened (Table 1). In addition to a decrease in most lipids, such as phospholipids, sphingolipids, and acyl-carnitines, a significant reduction in purine derivatives, such as AMP, adenosine 5′-diphosphate (ADP), and dGMP, were also noted in the plasma of SOD1^{G93A} mice.

Table 1
Differential metabolites between WT and SOD1^{G93A} mice in plasma at the pre-symptomatic stage.

Metabolites	WT_60	SOD1^{G93A}_60	*p* value	Metabolites	WT_60	SOD1^{G93A}_60	*p* value
13-Cis-acitretin	5.614	4.929	0.045	LPC 17:0 sn-1	0.009	0.007	0.004
dGMP	0.052	0.025	0.037	LPC O-18:0	0.012	0.011	0.035
N-formyl-L-methionine	0.007	0.004	0.012	Sphingosine-1-phosphate	0.121	0.109	0.037
AMP	0.157	0.099	0.045	8[R]-HETE	0.143	0.104	0.049
ADP	0.008	0.006	0.036	PC (33:1)	0.007	0.005	0.009
Carnitine C12:0	0.006	0.004	0.034	PC (33:2)	0.052	0.040	0.007
Carnitine C14:2	0.005	0.003	0.010	PC (31:0)	0.003	0.003	0.013
Carnitine C18:0	0.003	0.002	0.042	PE (38:3)	0.027	0.023	0.022
Cer(d18:1/24:1)-9a	0.001	0.001	0.039	PE (38:4)	0.024	0.020	0.005
Indolelactic acid	3.477	4.212	0.030	SM (36:3)	0.002	0.001	0.037
Leucine	3.109	3.745	0.035	LPE 16:0	0.028	0.031	0.023
LPC 15:0	0.027	0.022	0.003	AMP	0.157	0.099	0.045

dGMP = 2′-Deoxyguanosine 5′-monophosphate; AMP = Adenosine 5′-monophosphate; ADP = Adenosine 5′-diphosphate; Cer = Ceramides; LPC = Lysophosphatidylcholine; PC = Phosphatidylcholine; PE = Phosphatidylethanolamine; SM = Sphingomyelin; LPE = Lysophosphatidylethanolamine; AMP = Adenosine 5′-monophosphate; 8[R]-HETE = 8(R)-Hydroxy-(5Z,9E,11Z,14Z)-eicosatetraenoic acid.

For tissues, a visible regional difference was observed between the spinal cord and the motor cortex. In addition, the metabolic difference between SOD1^{G93A} mice and WT mice was more pronounced in the spinal cord than in the motor cortex (Fig. 3B). We then focused on the metabolic alterations in the spinal cord, and 20 DEMs were found to be significantly altered in SOD1^{G93A} mice (Table 2). Significant reductions in amino acids such as arginine, ornithine, and tyrosine were noted, with the exception of S-lactoylglutathione. In addition, we found a marked alteration in purine and its

derivatives (inosine, hypoxanthine, oxypurinol, AMP, ADP, and dGMP) in the spinal cord of SOD1^{G93A} mice. Although the trends of purine derivatives (AMP, ADP, and dGMP) in the plasma and spinal cord were inconsistent, disturbances in purine metabolism were found in both the central and peripheral circulation, suggesting that purine metabolism may have been disrupted in the early stage of ALS. More importantly, altered levels of a series of purine metabolites and disturbed purine metabolism were also found in the symptomatic stage, demonstrating the significance of purine metabolism in the development and progression of ALS.

Table 2
Differential metabolites between WT and SOD1^{G93A} mice in spinal cord at the pre-symptomatic stage.

Metabolites	WT_60	SOD1^{G93A}_60	SOD1^{G93A}/WT	*p* value	Metabolites	WT_60	SOD1^{G93A}_60	SOD1^{G93A}/WT	*p* value
AMP	1.083	1.547	1.428	0.002	Cysteine-glutathione disulfide	0.008	0.004	0.578	0.024
FFA C20:3	0.002	0.002	0.801	0.003	Tyrosine	0.000	0.000	0.841	0.020
Inosine	0.050	0.030	0.594	0.003	ADP	0.207	0.245	1.180	0.020
dGMP	0.005	0.009	1.775	0.004	Arginine	0.014	0.010	0.738	0.026
Hypoxanthine	0.318	0.237	0.748	0.004	Oxypurinol	0.000	0.000	0.689	0.026
UMP	0.000	0.000	1.422	0.005	N-acetyl-L-histidine	0.001	0.001	0.848	0.049
Methionine	0.004	0.003	0.752	0.007	Phenylalanine	0.008	0.007	0.882	0.026
Saccharopine	0.003	0.002	0.745	0.010	S-lactoyglutathione	0.002	0.003	1.595	0.035
Ornithine	0.000	0.000	0.778	0.011	FFA C20:2	0.003	0.003	0.844	0.043
Indoline	0.018	0.016	0.877	0.018					

AMP = Adenosine 5′-monophosphate; FFA= Free fatty acids; dGMP = 2′-Deoxyguanosine 5′-monophosphate; UMP = Uridine monophosphate.

Levels of the differentially expressed purine and purine derivatives in the spinal cord at different stages are presented in Fig. 3C–N. The results show that levels of adenine and its three derivatives (AMP, ADP, and ATP) increased at the pre-symptomatic stage and decreased at the symptomatic in SOD1^{G93A} mice (Fig. 3C–F). The same trend was observed in the alteration of four guanosine derivatives (cGMP, GDP, dGMP, and 2′-deoxyguanosine) (Fig. 3G–J). In contrast, the trend of inosine and hypoxanthine, uric acid, and allantoic acid were inconsistent with these results. Inosine and hypoxanthine were significantly reduced at the pre-symptomatic stage; however, no significant alteration was found at the symptomatic stage of ALS (Fig. 3K–L). The levels of uric acid and allantoic acid were significantly altered at the symptomatic stage. As an end-product of purine metabolism, the level of uric acid was significantly increased, whereas the level of allantoic acid, the oxidative product of uric acid, was significantly decreased in SOD1^{G93A} mice (Fig. 3M-N).

Proteomic analysis of the spinal cord in the symptomatic stage

To further understand the regulatory network of disturbed metabolic pathways and to unveil the underlying mechanism of metabolic alterations in ALS, the spinal cord samples from 120-day-old SOD1^{G93A} mice and WT littermates were subjected to proteomic analysis. According to the PCA analysis, the proteomes of WT and SOD1^{G93A} mice could be clearly discriminated (Fig. 4A). In total, 297 proteins were screened as differentially expressed proteins (DEPs) in WT and SOD1^{G93A} mice ($p < 0.05$, FDR < 0.1, fold change > 1.2). Of these proteins, 193 DEPs were upregulated, while 104 DEPs were downregulated (Fig. 4B **and Table S5**).

To interpret the biological significance of these DEPs, we performed the Gene Ontology (GO) annotation analysis, which depicts protein functions in three categories: biological processes (BP), molecular functions (MF), and cellular components (CC) (Fig. 4C). In terms of CC, these DEPs were mostly found in the cytosol or on mitochondria, ribosomes, synapses, and myelin sheaths. The analysis results of MF show that differential proteins were primarily associated with protein binding, macromolecular complex binding, and structural constituent of ribosome. The most correlated BP of the DEPs were translation, mitochondrial respiratory chain complex I assembly, fatty acid beta-oxidation, fatty acid metabolic process, etc. To further investigate the functions and signaling pathways that the DEPs were involved in, KEGG enrichment analysis were performed. In total, 93 KEGG pathways were enriched by 297 DEPs (**Table S6**), and the top 20 enriched pathways related to metabolism are shown as a bubble plot in Fig. 4D. These DEPs were found to be mainly associated with metabolic pathways such as oxidative phosphorylation, fatty acid metabolism, fatty acid degradation, and carbon metabolism. Moreover, some of these DEPs in the spinal cord were involved in the regulation of purine metabolism, which was found to be significantly disrupted in metabolomic analysis.

Table 3
Cluster details of MCODE protein-protein interaction and involved pathways.

Cluster	Score	Nodes	Edges	KEGG Pathways
1	24.56	26	614	Ribosome, RNA transport
2	12.5	13	150	Oxidative phosphorylation, Thermogenesis, Retrograde endocannabinoid signaling, and etc.
3	7.75	9	62	Spliceosome
4	4.889	28	132	Fatty acid metabolism, Peroxisome, Biosynthesis of unsaturated fatty acids, and etc.

To investigate the interactions among these DEPs, the STRING database was employed to construct a protein-protein interaction (PPI) network with a medium confidence level (0.4). The established PPI network consisted of 297 nodes and 1447 edges (**Table S7**). MCODE method was then applied with the default parameters (degree cutoff ≥ 2, node score cutoff ≥ 0.2, K-core ≥ 2, and max. depth = 100) to identify core modules in the established PPI network, following which seven clusters were found (scores > 3 and the number of nodes > 5) (**Table S8**). Proteins in the first four significant clusters were subjected to KEGG pathway enrichment analysis (Fig. 5A **and** Table 3). Cluster 1, including 26 nodes and 614 edges, was significantly enriched in the ribosome and RNA transport. Cluster 2, including 13 nodes and 150 edges, was markedly enriched in oxidative phosphorylation, thermogenesis, and retrograde endocannabinoid signaling. Proteins in Cluster 3 were involved in the spliceosome. The most correlated categories of Cluster 4 were fatty acid metabolism, peroxisome, and biosynthesis of unsaturated fatty acids (Table 3 and **Table S9**).

Oxidative phosphorylation is the process by which ATP is produced, coupled with the transport of electrons driven by five protein complexes (Complexes I–V) [32]. In our study, levels of eight nicotinamide adenine dinucleotide hydride (NADH) dehydrogenase (Complex I) subunits, two cytochrome C oxidase (Complex IV) subunits, and two ATP synthase (Complex V) subunits were found to be significantly reduced (Fig. 5B), suggesting impaired oxidative phosphorylation in $SOD1^{G93A}$ mice in the symptomatic stage. Meanwhile, DEPs involved in multiple FFA metabolism pathways were significantly elevated, indicating enhanced synthesis and utilization of FFAs (Fig. 5C).

Joint pathway analysis of proteomics and metabolomics

Since cellular metabolic activities could be regulated directly by proteins, and the concentration of metabolites could influence protein function and expression in turn, the joint pathway analysis of proteomics and metabolomics data was performed. The results show that DEPs and DEMs in the spinal cord of $SOD1^{G93A}$ mice in the symptomatic stage were simultaneously involved in metabolic pathways such as purine metabolism, tricarboxylic acid (TCA) cycle, arginine, proline metabolism, and fatty acid degradation ($p < 0.05$, Fig. 6 **and Table S10**). To visualize these changes at the metabolic and proteomic levels and their associations, we mapped the most important DEMs and DEPs into metabolic pathways (Fig. 7). Many purine metabolites were found to be altered in the spinal cord of $SOD1^{G93A}$ mice at both pre-symptomatic and symptomatic stages. Meanwhile, abnormal expressions of proteins involved in purine metabolism (PRPS2, ENTPD2, AMPD3, and NT5C) were also observed in the symptomatic stage. Moreover, expression levels of TCA cycle-related enzymes (ACLY, DLST, SUCLA2, and MDH2) were significantly reduced, while enzymes involved in fatty acid metabolism (HADHA, HADHB, ACADM, ACAA1, ACADSB, and ACOT1) were significantly increased in the spinal cord of $SOD1^{G93A}$ mice.

Discussion

In this study, the metabolic changes in plasma, spinal cord, and cortex during ALS evolution in $SOD1^{G93A}$ mice and age-matched littermates were investigated using unbiased comparative metabolomics analysis. Our findings indicate that $SOD1^{G93A}$ mice presented different metabolic signatures from WT mice starting in the pre-symptomatic stage, mainly involving lipid and purine metabolism. In the symptomatic stage, metabolic changes in the central nervous system and peripheral circulation were much more prominent. To further elucidate the mechanisms and regulatory network underlying the metabolic reprogramming in ALS, the lumbar spinal cords from symptomatic $SOD1^{G93A}$ mice and their littermates were collected and subjected to proteomics analysis. The results of GO annotation and KEGG enrichment analysis indicate that DEPs between $SOD1^{G93A}$ mice and WT mice were mainly located in mitochondria and involved in the process of mitochondrial respiratory chain complex I assembly, fatty acid beta-oxidation, oxidative phosphorylation, and fatty acid metabolic processes. More importantly, DEPs that were markedly enriched in oxidative phosphorylation and fatty acid metabolism were found to form highly interconnected network regions by MCODE analysis in the PPI network, further demonstrating the importance of oxidative phosphorylation and fatty acid metabolism in the development of ALS. Concomitantly, the joint pathway analysis of proteomics and metabolomics revealed that the most affected metabolic pathways in the symptomatic stage of ALS were purine metabolism, TCA cycle, arginine and proline metabolism, and fatty acid degradation.

Purine metabolism

For the first time, we found dysregulation in purine metabolism in the plasma and spinal cord of $SOD1^{G93A}$ mice at the pre-symptomatic stage. Moreover, our integrative analysis of metabolomics and proteomics identified purine metabolism as the most significant disrupted pathway in the spinal cord of $SOD1^{G93A}$ mice at the symptomatic stage. Purine and its derivatives are the basic blocks of bioenergetics, regulating cellular energy homeostasis and nucleotide synthesis [33]. Accumulative evidence suggests that purine metabolism plays an important role in the regulation of glial cell activation, the prevention of oxidative damage, and the modulation of glutamate transport [34–42]. An earlier *in vitro* study proved that astrocytes

carrying SOD1 mutation had abnormal alterations in inosine, adenosine, and cyclic adenosine monophosphate (cAMP) [43]. Inosine, guanosine, guanine, and adenine levels were also disrupted in the mitochondria plus the endoplasmic reticulum fraction of fibroblasts from ALS patients [44].

ATP, one of the most pivotal purine metabolites, can provide energy by hydrolyzing to ADP and AMP and exerts an important role in neuronal activation and inhibition [33, 45]. The majority of ATP required for cell activity is generated in mitochondria via oxidative phosphorylation. In our study, we found altered ADP, AMP, and adenine levels in the spinal cords of $SOD1^{G93A}$ mice at the pre-symptomatic stage, before microglia activation and disease onset. ATP is normally released by astrocytes and neurons, and it can regulate the function of neurons, astrocytes, oligodendrocytes, and microglia by binding to P2 or P1 purinergic receptors, thus influencing the response to inflammation, calcium signaling, and synaptic activity [34–36]. Statistics show that neuronal injury can cause an abnormal release of ATP and its catabolites, which then cause neuroinflammation and astrogliosis by activating microglia and astrocytes [37–38].

Glutamate-induced excitotoxicity-mediated motor neuron degeneration is one of the major hypotheses for the pathogenesis of ALS [46]. Guanosine 5'-triphosphate (GTP), GDP, GMP, and guanosine could interact with vesicular glutamate carriers in vitro [39]. Guanosine could also protect neurons from glutamate-induced toxicity by promoting glutamate uptake and inhibiting glutamate release [40–42]. More importantly, second messenger molecules such as cAMP and cyclic guanosine monophosphate (cGMP) have been shown to have an effect on the activation of proteasomes and promote the degradation of misfolded and mutated proteins without interfering with autophagy [47–48]. Impaired protein homeostasis and accumulation of misfolded proteins are considered two of the fundamental pathologic features of ALS [49–50]. There is evidence suggesting that the phosphodiesterase 5 (PDE5) inhibitor-induced increase in cGMP can promote the degradation of mutant tau and mutant huntingtin, thereby improving neuronal death and morphological abnormalities [48]. According to our findings, the level of cGMP in ALS mice significantly diminished during the symptomatic stage. Thus, strategies aimed at increasing the level of cGMP might be a potential therapeutic intervention for ALS.

Furthermore, in $SOD1^{G93A}$ mice, we found an elevated level of uric acid, the end product of purines, and a reduced level of its oxidative product, allantoic acid, at the symptomatic stage. The protective effect of uric acid has been reported in neurodegenerative diseases. It was reported that uric acid could protect dopaminergic neurons from death by reducing reactive oxygen species (ROS) production and protein oxidation, which was dependent on the presence of astrocytes [51]. Uric acid also helped to eliminate excess extracellular glutamate by enhancing the expression of glutamate transporter excitatory amino acid transporter 1 (EAAT-1) in astrocytes [52]. These findings emphasize the strong link between purine metabolism and ALS pathogenesis. Thus, further investigation into the role of purine metabolism in the development of ALS may aid in the discovery of early biomarkers and novel therapeutic targets for clinical intervention.

Fatty acid metabolism

Marked upregulation of proteins involved in FFA biosynthesis and degradation and elevation of FFAs in plasma both demonstrated an enhanced FFA metabolism in ALS mice. Hypermetabolism is a common feature of ALS, with up to 60% of patients being hypermetabolic [53]. Hypermetabolism could cause a mobilization of peripheric lipid stores, resulting in significant reductions in fat mass and increased FFA metabolism [53–54]. Since the pre-symptomatic stage, the SOD1 mice model shows increased metabolism and decreased body weight independent of energy intake [55]. Several studies have suggested that increased fat utilization in ALS might be associated with increased energy expenditure caused by muscle atrophy and the degeneration of sympathetic nerve innervation of adipose tissue [55–58]. Furthermore, decreased energy production resulting from mitochondria abnormalities, increased release of pro-inflammatory cytokines and accumulated ROS might also be responsible [55, 59–60]. A previous study reported that glucose metabolism was downregulated and the respiratory exchange ratio was significantly lower in SOD1 mice, indicating increased FFA oxidation [61]. Excessive FFA metabolism has been linked to complex pro-inflammatory factors [62], which can activate the p38 signaling pathway via ROS production, leading to progressive muscle wasting [63–64]. In addition, increased AMP-activated protein kinase (AMPK) activation was reported in motor neurons generated from the spinal cord of SOD1 mice and ALS patients [65–68]. The activation of AMPK may promote FFA oxidation by phosphorylating acetyl-CoA carboxylase [61].

Previous studies found that inhibition of FFA oxidation could attenuate excessive energy expenditure and improve energy metabolism by increasing muscle ATP content in $SOD1^{G93A}$ mice [61–62]. In ALS patients, a close relationship between serum lipid profile and survival has been found [69]. Higher levels of ω-3 polyunsaturated fatty acids (PUFAs) were thought to protect against ALS [70]. Increased levels of FFAs, such as palmitoleate and oleate, in blood, have also been linked to prolonged survival [71]. Docosahexaenoic acid (DHA) supplementation was found to reduce circulating pro-inflammatory cytokine TNF-α and DNA oxidative damage and increase the survival of male $SOD1^{G93A}$ mice by 7% [72]. These findings demonstrate that targeting FFA metabolism might provide new strategies for better ALS management.

TCA cycle and oxidative phosphorylation

To maintain basic physiological functions, such as action potentials and postsynaptic signaling, the central nervous system requires approximately 20% of the body's energy [73–75]. This energy is gradually generated via glycolysis, the TCA cycle, and mitochondrial oxidative phosphorylation processes [7]. Proteins implicated in glycolysis and the TCA cycle have been found to have abnormal expressions in both ALS patients and $SOD1^{G93A}$ mice [76–77]. In our study, we found increased expressions of glucose-6-phosphate and fructose-1,6-bisphosphate in the spinal cords of $SOD1^{G93A}$ mice at the symptomatic stage, further indicating a defect in glycolysis in ALS. Impaired glycolysis might lead to a reduced entry of pyruvate into the TCA cycle [78]. In $SOD1^{G93A}$ mice, reduced gene expressions of isocitrate dehydrogenase, oxoglutarate dehydrogenase, and malate dehydrogenase 1 (MDH1) were reported, which was consistent with our results from proteomics [79–81]. Previously, elevated succinate, one of the intermediates of the

TCA cycle, was found in ALS patients [82]. Consistently, we noted an accumulated level of cis-aconitate in our study. These findings might indicate decreased activities of related enzymes and inhibition of the TCA cycle in ALS. It was documented that, in isolated nerve terminals and various cellular systems, reduced activities of TCA cycle enzymes were associated with the elevation of oxidative stress [16, 83–84]. Additionally, aggregation of mutated SOD1 proteins might also impair the TCA cycle by interfering with malate-aspartate shuttle activity in the mitochondrial membrane [85–86].

The inhibition of the TCA cycle could not only lead to the reduction in the acetyl-CoA but also affect the generation of NADP and electrons, ultimately resulting in the dysfunction of oxidative phosphorylation [83–84]. In the blood cells of ALS patients, the mRNA level of succinate dehydrogenase complex (Complex II) subunit B was reduced [87]. Besides, the activities of Complexes I and III as well as Complex IV were diminished in the spinal cord of ALS patients [88]. Our data here clearly show that the expressions of eight subunits of NADH dehydrogenase (Complex I), two subunits of cytochrome C oxidase (Complex IV), and two subunits of ATP synthase (Complex V) were significantly reduced in the symptomatic stage, revealing the detailed alteration of these three complexes. More importantly, these subunits clustered significantly in the PPI network established by DEPs between $SOD1^{G93A}$ mice and WT mice, further demonstrating the essential role of oxidative phosphorylation in ALS pathogenesis. Notably, in another study, ATP synthase expression was found to be elevated in the pre-symptomatic stage, which could be a compensatory change to meet increased energy demand at the early stage [89]. It is known that inadequate ATP production aggravates mitochondrial dysfunction and contributes to motor neuron death [90–91]. Improved glycolysis or TCA cycle by enhancing pyruvate dehydrogenase activity or replenishing TCA cycle intermediates has been shown in studies to prolong disease duration by improving mitochondrial function [92–93].

Conclusion

This study investigated the metabolic changes in both the central nervous system and peripheral circulation of $SOD1^{G93A}$ mice at different stages of ALS, emphasizing the importance of metabolic alterations in the longitudinal development of ALS pathophysiology. Specifically, the present study demonstrated that both plasma and spinal cord at the pre-symptomatic stage had a distinct metabolic profile, compared to the symptomatic stage, especially in lipid and purine metabolism. Moreover, proteomics analysis was performed on the major lesion site (spinal cord). Based on the integrative analysis, we highlighted that the abnormalities of purine metabolism, fatty acid metabolism, TCA cycle, and oxidative phosphorylation are crucial events in ALS pathophysiology. Our results complement existing data on metabolic reprogramming in ALS and provide new insights into the discovery of reliable early diagnostic biomarkers and therapeutic targets for ALS.

Abbreviations

ALS	Amyotrophic lateral sclerosis
SOD1	Superoxide dismutase 1
LC-MS	Liquid chromatography–mass spectrometry
RSD	Relative standard deviation
QC	Quality control
PCA	Principal component analysis
SD	Standard deviation
OPLS-DA	Orthogonal partial least-squares discrimination analysis
VIP	Variable importance in the projection
FFA	Free fatty acids
PC	Phosphatidylcholine
LPC	Lysophosphatidylcholine
PE	Phosphatidylethanolamine
LPE	Lysophosphatidylethanolamine
AMP	Adenosine 5’-monophosphate
ADP	Adenosine 5’-diphosphate
ATP	Adenosine 5’-triphosphate
GDP	Guanosine 5’-diphosphate

GTP	Guanosine 5′-triphosphate
cGMP	Guanosine 3′,5′-cyclic monophosphate
dGMP	2′-Deoxyguanosine 5′-monophosphate
PLS-DA	Partial least-squares discrimination analysis
DEPs	Differentially expressed proteins
GO	Gene Ontology
BP	Biological processes
MF	Molecular functions
CC	Cellular components
PPI	Protein-protein interaction
PRPS2	Phosphoribosyl pyrophosphate synthetase 2
ENTPD2	Ectonucleoside triphosphate diphosphohydrolase 2
AMPD3	Adenosine monophosphate deaminase 3
NT5C	5′,3′-nucleotidase, cytosolic
ROS	Reactive oxygen species
PDE5	Phosphodiesterase 5
AMPK	Adenosine 5′-monophosphate-activated protein kinase
ACLY	ATP citrate lyase
DLST	Succinyltransferase
SUCLA2	Succinate-CoA ligase
MDH	Malate dehydrogenase
WT	Wildtype
TCA	Tricarboxylic acid
NADH	Nicotinamide adenine dinucleotide hydride
MCODE	Molecular complex detection
KEGG	Kyoto encyclopedia of genes and genomes
cAMP	Cyclic adenosine monophosphate
EAAT-1	Excitatory amino acid transporter 1
AMPK	AMP-activated protein kinase
PUFAs	Polyunsaturated fatty acids
DHA	Docosahexaenoic acid

Declarations

Ethics approval and consent to participate

All experiments were carried out in accordance with Institutional Animal Care and Use Committee guidelines. The Ethical Committee of Dalian Medical University approved all the animal experiments and procedures.

Consent for publication

Not applicable.

Availability of data and materials

The dataset(s) supporting the conclusions of this article is(are) included within the article (and its additional file(s)), further inquiries can be directed to the corresponding author/s.

Competing interests

The authors declare that they have no competing interests.

Funding

This work was supported by funding from the National Natural Sciences Foundation of China (NSFC 22004013), the National Key Research and Development Program of China (2016YFC1306600), Key R & D Program of Guangdong Provincial (2018B030337001), Doctoral Scientific Research Foundation of Liaoning Science and Technology Department (2020-BS-200) and the Central Guidance on Local Science and Technology Development Fund of Dalian Science and Technology Bureau.

Author Contributions

Authors' contributions are as follows: Weidong Le and Guowang Xu designed the study; Xiaojiao Xu and Yaping Shao draft the manuscript, Xiaojiao Xu, Yaping Shao, Qiu Yang and Manli Wang performed the metabolomics and data analysis; Zheyi Liu performed the proteomics analysis; Hang Yu, Rong Zhang and Sheng Chen helped with editing and modifying the manuscript. All the authors read and approved the manuscript.

Acknowledgments

Not applicable.

References

1. Gordon PH, Cheng B, Katz IB, Mitsumoto H, Rowland LP. Clinical features that distinguish PLS, upper motor neuron-dominant ALS, and typical ALS. Neurology. 2009;72:1948–52.
2. Oskarsson B, Gendron TF, Staff NP. Amyotrophic Lateral Sclerosis: An Update for 2018. Mayo Clin Proc. 2018, 93, 1617–1628.
3. Norris SP, Likanje MN, Andrews JA. Amyotrophic lateral sclerosis: update on clinical management. Curr Opin Neurol. 2020;33:641–8.
4. Xu X, Shen D, Gao Y, Zhou Q, Ni Y, Meng H, et al. A perspective on therapies for amyotrophic lateral sclerosis: can disease progression be curbed? Translational neurodegeneration. 2021;10:29.
5. Morello G, Salomone S, D'Agata V, Conforti FL, Cavallaro S. From Multi-Omics Approaches to Precision Medicine in Amyotrophic Lateral Sclerosis. Front Neurosci. 2020;14:577755.
6. Vandoorne T, De Bock K, Van Den Bosch L. Energy metabolism in ALS: an underappreciated opportunity? Acta Neuropathol., 2018, 135, 489–509.
7. Tefera TW, Steyn FJ, Ngo ST, Borges K. CNS glucose metabolism in Amyotrophic Lateral Sclerosis: a therapeutic target? Cell & bioscience. 2021;11:14.
8. Dupuis L, Pradat PF, Ludolph AC, Loeffler JP. Energy metabolism in amyotrophic lateral sclerosis. Lancet Neurol. 2011;10:75–82.
9. Huisman MH, Seelen M, van Doormaal PT, de Jong SW, de Vries JH, van der Kooi AJ, et al. Effect of Presymptomatic Body Mass Index and Consumption of Fat and Alcohol on Amyotrophic Lateral Sclerosis. JAMA Neurol. 2015;72:1155–62.
10. Mariosa D, Beard JD, Umbach DM, Bellocco R, Keller J, Peters TL, et al. Body Mass Index and Amyotrophic Lateral Sclerosis: A Study of US Military Veterans. Am J Epidemiol. 2017;185:362–71.
11. Dorst J, Kühnlein P, Hendrich C, Kassubek J, Sperfeld AD, Ludolph AC. Patients with elevated triglyceride and cholesterol serum levels have a prolonged survival in amyotrophic lateral sclerosis. J Neurol. 2011;258:613–7.
12. Blasco H, Veyrat-Durebex C, Bocca C, Patin F, Vourc'h P, Kouassi Nzoughet J, et al. Lipidomics Reveals Cerebrospinal-Fluid Signatures of ALS. Sci Rep. 2017;7:17652.
13. Dalakas MC, Hatazawa J, Brooks RA, Di Chiro G. Lowered cerebral glucose utilization in amyotrophic lateral sclerosis. Ann Neurol. 1987;22:580–6.
14. Weerasekera A, Crabbé M, Tomé SO, Gsell W, Sima D, Casteels C, et al. Non-invasive characterization of amyotrophic lateral sclerosis in a hTDP-43(A315T) mouse model: A PET-MR study. NeuroImage. Clinical. 2020;27:102327.
15. Goutman SA, Boss J, Guo K, Alakwaa FM, Patterson A, Kim S, et al. Untargeted metabolomics yields insight into ALS disease mechanisms. J Neurol Neurosurg Psychiatry. 2020;91:1329–38.
16. Tefera TW, Bartlett K, Tran SS, Hodson MP, Borges K. Impaired Pentose Phosphate Pathway in the Spinal Cord of the hSOD1(G93A) Mouse Model of Amyotrophic Lateral Sclerosis. Mol Neurobiol. 2019;56:5844–55.

17. Patin F, Corcia P, Vourc'h P, Nadal-Desbarats L, Baranek T, Goossens JF, et al. Omics to Explore Amyotrophic Lateral Sclerosis Evolution: the Central Role of Arginine and Proline Metabolism. Mol Neurobiol. 2017;54:5361–74.
18. Bjornevik K, O'Reilly ÉJ, Berry JD, Clish CB, Jeanfavre S, Kato I, et al. Prediagnostic plasma branched-chain amino acids and the risk of amyotrophic lateral sclerosis. Neurology. 2019;92:e2081–8.
19. Pharaoh G, Sataranatarajan K, Street K, Hill S, Gregston J, Ahn B, et al. Metabolic and Stress Response Changes Precede Disease Onset in the Spinal Cord of Mutant SOD1 ALS Mice. Front Neurosci. 2019;13:487.
20. Karczewski KJ, Snyder MP. Integrative omics for health and disease. Nat Rev Genet. 2018;19:299–310.
21. Wishart DS. Metabolomics for Investigating Physiological and Pathophysiological Processes. Physiol Rev. 2019;99:1819–75.
22. Weckwerth W, Morgenthal K. Metabolomics: from pattern recognition to biological interpretation. Drug Discovery Today. 2005;10:1551–8.
23. Gurney ME, Pu H, Chiu AY, Dal Canto MC, Polchow CY, Alexander DD, et al. Motor neuron degeneration in mice that express a human Cu,Zn superoxide dismutase mutation. Science. 1994;264:1772–5.
24. Zhang X, Li L, Chen S, Yang D, Wang Y, Zhang X, et al. Rapamycin treatment augments motor neuron degeneration in SOD1(G93A) mouse model of amyotrophic lateral sclerosis. Autophagy. 2011;7:412–25.
25. Huang Y, Chen G, Liu X, Shao Y, Gao P, Xin C, et al. Serum metabolomics study and eicosanoid analysis of childhood atopic dermatitis based on liquid chromatography-mass spectrometry. J Proteome Res. 2014;13:5715–23.
26. Luo P, Yin P, Hua R, Tan Y, Li Z, Qiu G, et al. A Large-scale, multicenter serum metabolite biomarker identification study for the early detection of hepatocellular carcinoma. Hepatology. 2018;67:662–75.
27. Ren S, Shao Y, Zhao X, Hong CS, Wang F, Lu X, et al. Integration of Metabolomics and Transcriptomics Reveals Major Metabolic Pathways and Potential Biomarker Involved in Prostate Cancer. Mol Cell Proteomics. 2016;15:154–63.
28. Zhao X, Zeng Z, Chen A, Lu X, Zhao C, Hu C, et al. Comprehensive Strategy to Construct In-House Database for Accurate and Batch Identification of Small Molecular Metabolites. Anal Chem. 2018;90:7635–43.
29. Smilde AK, van der Werf MJ, Bijlsma S; van der Werff-van der Vat BJ, Jellema RH. Fusion of mass spectrometry-based metabolomics data. Anal Chem, 2005, 77, 6729–36.
30. Wang S, Li W, Hu L, Cheng J, Yang H, Liu Y. NAguideR: performing and prioritizing missing value imputations for consistent bottom-up proteomic analyses. Nucleic Acids Res. 2020;48:e83.
31. Zhang X, Chen S, Li L, Wang Q, Le W. Decreased level of 5-methyltetrahydrofolate: a potential biomarker for pre-symptomatic amyotrophic lateral sclerosis. J Neurol Sci. 2010;293:102–5.
32. Thomsen GM, Gowing G, Latter J, Chen M, Vit JP, Staggenborg K, et al. Delayed disease onset and extended survival in the SOD1G93A rat model of amyotrophic lateral sclerosis after suppression of mutant SOD1 in the motor cortex. J Neurosci. 2014;34:15587–600.
33. Huang Z, Xie N, Illes P, Di Virgilio F, Ulrich H, Semyanov A, et al. From purines to purinergic signalling: molecular functions and human diseases. Signal Transduct Target therapy. 2021;6:162.
34. Allen SP, Hall B, Castelli LM, Francis L, Woof R, Siskos AP, et al. Astrocyte adenosine deaminase loss increases motor neuron toxicity in amyotrophic lateral sclerosis. Brain. 2019;142:586–605.
35. Larsson M, Sawada K, Morland C, Hiasa M, Ormel L, Moriyama Y, et al. Functional and anatomical identification of a vesicular transporter mediating neuronal ATP release. Cereb Cortex. 2012;22:1203–14.
36. Abbracchio MP, Burnstock G, Verkhratsky A, Zimmermann H. Purinergic signalling in the nervous system: an overview. Trends Neurosci. 2009;32:19–29.
37. Di Virgilio F, Ceruti S, Bramanti P, Abbracchio MP. Purinergic signalling in inflammation of the central nervous system. Trends Neurosci. 2009;32:79–87.
38. Fields RD, Burnstock G. Purinergic signalling in neuron-glia interactions. Nat Rev Neurosci. 2006;7:423–36.
39. Tasca CI, Santos TG, Tavares RG, Battastini AM, Rocha JB, Souza DO. Guanine derivatives modulate L-glutamate uptake into rat brain synaptic vesicles. Neurochem Int. 2004;44:423–31.
40. Molz S, Dal-Cim T, Budni J, Martín-de-Saavedra MD, Egea J, Romero A, et al. Neuroprotective effect of guanosine against glutamate-induced cell death in rat hippocampal slices is mediated by the phosphatidylinositol-3 kinase/Akt/ glycogen synthase kinase 3β pathway activation and inducible nitric oxide synthase inhibition. J Neurosci Res. 2011;89:1400–8.
41. Dal-Cim T, Ludka FK, Martins WC, Reginato C, Parada E, Egea J, et al. Guanosine controls inflammatory pathways to afford neuroprotection of hippocampal slices under oxygen and glucose deprivation conditions. J Neurochem. 2013;126:437–50.
42. Dal-Cim T, Martins WC, Santos AR, Tasca CI. Guanosine is neuroprotective against oxygen/glucose deprivation in hippocampal slices via large conductance Ca^{2+}-activated K + channels, phosphatidilinositol-3 kinase/protein kinase B pathway activation and glutamate uptake. Neuroscience. 2011;183:212–20.
43. Madji Hounoum B, Mavel S, Coque E, Patin F, Vourc'h P, Marouillat S, et al. Wildtype motoneurons, ALS-Linked SOD1 mutation and glutamate profoundly modify astrocyte metabolism and lactate shuttling. Glia. 2017;65:592–605.

44. Veyrat-Durebex C, Bris C, Codron P, Bocca C, Chupin S, Corcia P, et al. Metabo-lipidomics of Fibroblasts and Mitochondrial-Endoplasmic Reticulum Extracts from ALS Patients Shows Alterations in Purine, Pyrimidine, Energetic, and Phospholipid Metabolisms. Mol Neurobiol. 2019;56:5780–91.
45. Todd KJ, Robitaille R. Purinergic modulation of synaptic signalling at the neuromuscular junction. Pflugers Arch. 2006;452:608–14.
46. Bendotti C, Carrì MT. Lessons from models of SOD1-linked familial ALS. Trends Mol Med. 2004;10:393–400.
47. Lokireddy S, Kukushkin NV, Goldberg AL. cAMP-induced phosphorylation of 26S proteasomes on Rpn6/PSMD11 enhances their activity and the degradation of misfolded proteins. Proc Natl Acad Sci U S A. 2015;112:E7176-85.
48. VerPlank JJS, Tyrkalska SD, Fleming A, Rubinsztein DC, Goldberg AL. cGMP via PKG activates 26S proteasomes and enhances degradation of proteins, including ones that cause neurodegenerative diseases. Proc Natl Acad Sci U S A. 2020;117:14220–30.
49. Chua JP, De Calbiac H, Kabashi E, Barmada SJ. Autophagy and ALS: mechanistic insights and therapeutic implications. Autophagy. 2022;18:254–82.
50. Karabiyik C, Frake RA, Park SJ, Pavel M, Rubinsztein DC. Autophagy in ageing and ageing-related neurodegenerative diseases. Ageing and Neurodegenerative Diseases. 2021;1:2.
51. Cipriani S, Desjardins CA, Burdett TC, Xu Y, Xu K, Schwarzschild MA. Protection of dopaminergic cells by urate requires its accumulation in astrocytes. J Neurochem. 2012;123:172–81.
52. Du Y, Chen CP, Tseng CY, Eisenberg Y, Firestein BL. Astroglia-mediated effects of uric acid to protect spinal cord neurons from glutamate toxicity. Glia. 2007;55:463–72.
53. Desport JC, Preux PM, Magy L, Boirie Y, Vallat JM, Beaufrère B, et al. Factors correlated with hypermetabolism in patients with amyotrophic lateral sclerosis. Am J Clin Nutr. 2001;74:328–34.
54. Badjatia N, Seres D, Carpenter A, Schmidt JM, Lee K, Mayer SA, et al. Free Fatty acids and delayed cerebral ischemia after subarachnoid hemorrhage. Stroke. 2012;43:691–6.
55. Dupuis L, Oudart H, René F, Gonzalez de Aguilar JL, Loeffler JP. Evidence for defective energy homeostasis in amyotrophic lateral sclerosis: benefit of a high-energy diet in a transgenic mouse model. Proc Natl Acad Sci U S A. 2004;101:11159–64.
56. Lindauer E, Dupuis L, Müller HP, Neumann H, Ludolph AC, Kassubek J. Adipose Tissue Distribution Predicts Survival in Amyotrophic Lateral Sclerosis. PLoS One. 2013;8:e67783.
57. Bachman ES, Dhillon H, Zhang CY, Cinti S, Bianco AC, Kobilka BK, et al. betaAR signaling required for diet-induced thermogenesis and obesity resistance. Science. 2002;297:843–5.
58. Muscaritoli M, Kushta I, Molfino A, Inghilleri M, Sabatelli M, Rossi Fanelli F. Nutritional and metabolic support in patients with amyotrophic lateral sclerosis. Nutrition. 2012;28:959–66.
59. Coppack SW. Pro-inflammatory cytokines and adipose tissue. Proc. Nutr. Soc., 2001, 60, 349 – 56.
60. Pan R, Chen Y. Management of Oxidative Stress: Crosstalk Between Brown/Beige Adipose Tissues and Skeletal Muscles. Front Physiol. 2021;12:712372.
61. Scaricamazza S, Salvatori I, Giacovazzo G, Loeffler JP, Renè F, Rosina M, et al. Skeletal-Muscle Metabolic Reprogramming in ALS-SOD1(G93A) Mice Predates Disease Onset and Is A Promising Therapeutic Target. iScience. 2020;23:101087.
62. Fukawa T, Yan-Jiang BC, Min-Wen JC, Jun-Hao ET, Huang D, Qian CN, et al. Excessive fatty acid oxidation induces muscle atrophy in cancer cachexia. Nat Med. 2016;22:666–71.
63. Bernet JD, Doles JD, Hall JK, Kelly Tanaka K, Carter TA, Olwin BB. p38 MAPK signaling underlies a cell-autonomous loss of stem cell self-renewal in skeletal muscle of aged mice. Nat Med. 2014;20:265–71.
64. Cosgrove BD, Gilbert PM, Porpiglia E, Mourkioti F, Lee SP, Corbel SY, et al. Rejuvenation of the muscle stem cell population restores strength to injured aged muscles. Nat Med. 2014;20:255–64.
65. Lim MA, Selak MA, Xiang Z, Krainc D, Neve RL, Kraemer BC, et al. Reduced activity of AMP-activated protein kinase protects against genetic models of motor neuron disease. J Neurosci. 2012;32:1123–41.
66. Perera ND, Sheean RK, Scott JW, Kemp BE, Horne MK, Turner BJ. Mutant TDP-43 deregulates AMPK activation by PP2A in ALS models. PLoS One. 2014;9:e90449.
67. Sui Y, Zhao Z, Liu R, Cai B, Fan D. Adenosine monophosphate-activated protein kinase activation enhances embryonic neural stem cell apoptosis in a mouse model of amyotrophic lateral sclerosis. Neural regeneration research. 2014;9:1770–8.
68. Liu YJ, Lee LM, Lai HL, Chern Y. Aberrant activation of AMP-activated protein kinase contributes to the abnormal distribution of HuR in amyotrophic lateral sclerosis. FEBS Lett. 2015;589:432–9.
69. Dupuis L, Corcia P, Fergani A, Gonzalez De Aguilar JL, Bonnefont-Rousselot D, Bittar R, et al. Dyslipidemia is a protective factor in amyotrophic lateral sclerosis. Neurology. 2008;70:1004–9.
70. Fitzgerald KC, O'Reilly ÉJ, Falcone GJ, McCullough ML, Park Y, Kolonel LN, et al. Dietary ω-3 polyunsaturated fatty acid intake and risk for amyotrophic lateral sclerosis. JAMA Neurol. 2014;71:1102–10.
71. Henriques A, Blasco H, Fleury MC, Corcia P, Echaniz-Laguna A, Robelin L, et al. Blood Cell Palmitoleate-Palmitate Ratio Is an Independent Prognostic Factor for Amyotrophic Lateral Sclerosis. PLoS One. 2015;10:e0131512.

72. Torres P, Cacabelos D, Pairada J, Bauer KC, Boada J, Fontdevila L, et al. Gender-Specific Beneficial Effects of Docosahexaenoic Acid Dietary Supplementation in G93A-SOD1 Amyotrophic Lateral Sclerosis Mice. Neurotherapeutics. 2020;17:269–81.
73. Ames A. 3rd. CNS energy metabolism as related to function. Brain Res Brain Res Rev. 2000;34:42–68.
74. Attwell D, Laughlin SB. An energy budget for signaling in the grey matter of the brain. J Cereb Blood Flow Metab. 2001;21:1133–45.
75. Bordone MP, Salman MM, Titus HE, Amini E, Andersen JV, Chakraborti B, et al. The energetic brain - A review from students to students. J Neurochem. 2019;151:139–65.
76. Ferraiuolo L, Higginbottom A, Heath PR, Barber S, Greenald D, Kirby J, et al. Dysregulation of astrocyte-motoneuron cross-talk in mutant superoxide dismutase 1-related amyotrophic lateral sclerosis. Brain. 2011;134:2627–41.
77. Wang XS, Simmons Z, Liu W, Boyer PJ, Connor JR. Differential expression of genes in amyotrophic lateral sclerosis revealed by profiling the post mortem cortex. Amyotroph Lateral Scler. 2006;7:201–10.
78. Tefera TW, Borges K. Neuronal glucose metabolism is impaired while astrocytic TCA cycling is unaffected at symptomatic stages in the hSOD1(G93A) mouse model of amyotrophic lateral sclerosis. J Cereb Blood Flow Metab. 2019;39:1710–24.
79. D'Arrigo A, Colavito D, Peña-Altamira E, Fabris M, Dam M, Contestabile A, et al. Transcriptional Profiling in the Lumbar Spinal Cord of a Mouse Model of Amyotrophic Lateral Sclerosis: A Role for Wild-Type Superoxide Dismutase 1 in Sporadic Disease? J Mol Neurosci. 2010;41:404–15.
80. Ferraiuolo L, Higginbottom A, Heath PR, Barber S, Greenald D, Kirby J, et al. Dysregulation of astrocyte–motoneuron cross-talk in mutant superoxide dismutase 1-related amyotrophic lateral sclerosis. Brain. 2011;134:2627–41.
81. Lederer CW, Torrisi A, Pantelidou M, Santama N, Cavallaro S. Pathways and genes differentially expressed in the motor cortex of patients with sporadic amyotrophic lateral sclerosis. BMC Genomics. 2007;8:26.
82. Wuolikainen A, Andersen PM, Moritz T, Marklund SL, Antti H. ALS patients with mutations in the SOD1 gene have an unique metabolomic profile in the cerebrospinal fluid compared with ALS patients without mutations. Mol Genet Metab. 2012;105:472–8.
83. Mailloux RJ, Bériault R, Lemire J, Singh R, Chénier DR, Hamel RD, et al. The tricarboxylic acid cycle, an ancient metabolic network with a novel twist. PLoS One. 2007;2:e690.
84. Tretter L, Adam-Vizi V. Inhibition of Krebs cycle enzymes by hydrogen peroxide: A key role of [alpha]-ketoglutarate dehydrogenase in limiting NADH production under oxidative stress. J Neurosci. 2000;20:8972–9.
85. Veyrat-Durebex C, Corcia P, Piver E, Devos D, Dangoumau A, Gouel F, et al. Disruption of TCA Cycle and Glutamate Metabolism Identified by Metabolomics in an In Vitro Model of Amyotrophic Lateral Sclerosis. Mol Neurobiol. 2016;53:6910–24.
86. Oladzad Abbasabadi A, Javanian A, Nikkhah M, Meratan AA, Ghiasi P, Nemat-Gorgani M. Disruption of mitochondrial membrane integrity induced by amyloid aggregates arising from variants of SOD1. Int J Biol Macromol. 2013;61:212–7.
87. Lin J, Diamanduros A, Chowdhury SA, Scelsa S, Latov N, Sadiq SA. Specific electron transport chain abnormalities in amyotrophic lateral sclerosis. J Neurol. 2009;256:774–82.
88. Wiedemann FR, Manfredi G, Mawrin C, Beal MF, Schon EA. Mitochondrial DNA and respiratory chain function in spinal cords of ALS patients. J Neurochem. 2002;80:616–25.
89. Ferraiuolo L, Heath PR, Holden H, Kasher P, Kirby J, Shaw PJ. Microarray analysis of the cellular pathways involved in the adaptation to and progression of motor neuron injury in the SOD1 G93A mouse model of familial ALS. J Neurosci. 2007;27:9201–19.
90. Cozzolino M, Carrì MT. Mitochondrial dysfunction in ALS. Prog Neurobiol. 2012;97:54–66.
91. Ravera S, Torazza C, Bonifacino T, Provenzano F, Rebosio C, Milanese M, et al. Altered glucose catabolism in the presynaptic and perisynaptic compartments of SOD1(G93A) mouse spinal cord and motor cortex indicates that mitochondria are the site of bioenergetic imbalance in ALS. J Neurochem. 2019;151:336–50.
92. Miquel E, Cassina A, Martínez-Palma L, Bolatto C, Trías E, Gandelman M, et al. Modulation of astrocytic mitochondrial function by dichloroacetate improves survival and motor performance in inherited amyotrophic lateral sclerosis. PLoS One. 2012;7:e34776.
93. Tefera TW, Wong Y, Barkl-Luke ME, Ngo ST, Thomas NK, McDonald TS, et al. Triheptanoin Protects Motor Neurons and Delays the Onset of Motor Symptoms in a Mouse Model of Amyotrophic Lateral Sclerosis. PLoS One. 2016;11:e0161816.

Figures

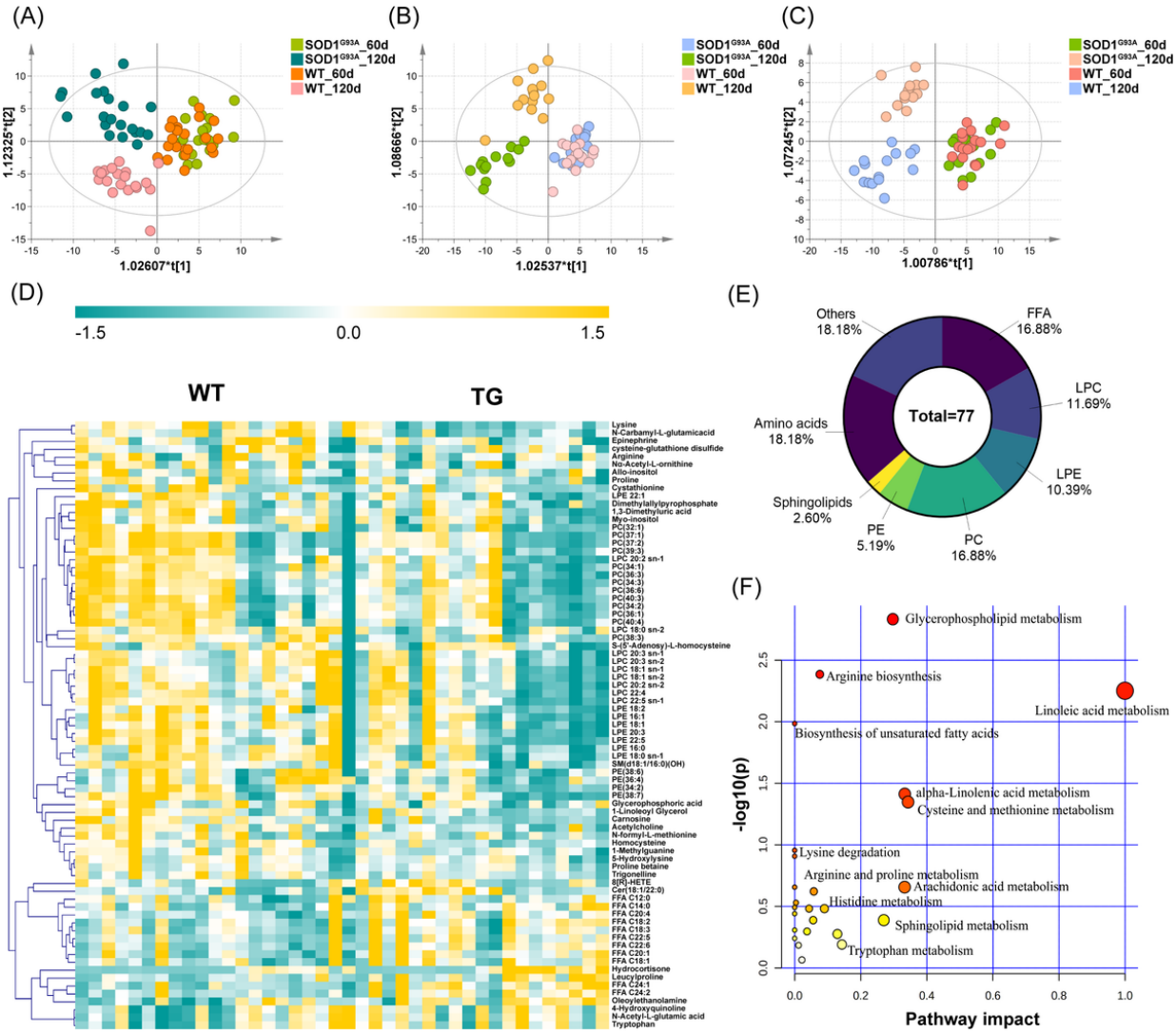


Figure 1

Metabolic signature of SOD1^{G93A} mice in plasma in the symptomatic stage. **(A)** OPLS-DA score plot of metabolome in plasma. Model parameters: R2X = 0.397, R2Y = 0.645, Q2 = 0.359. CV-ANOVA data: p = 0, F factor = 4.21. **(B)** OPLS-DA score plot of metabolome in spinal cord. Model parameters: R2X = 0.343, R2Y = 0.732, Q2 = 0.485. CV-ANOVA data: p = 0, F factor = 4.44. **(C)** OPLS-DA score plot of metabolome in cortex. Model parameters: R2X = 0.509, R2Y = 0.775, Q2 = 0.374. CV-ANOVA data: p = 0.0001, F factor = 2.43. **(D)** Heat map of the differential metabolites between WT and SOD1^{G93A} mice in plasma. **(E)** Distribution of each chemical class in all DEMs in plasma. (**F**) Pathway analysis of the differentially expressed metabolites in plasma.

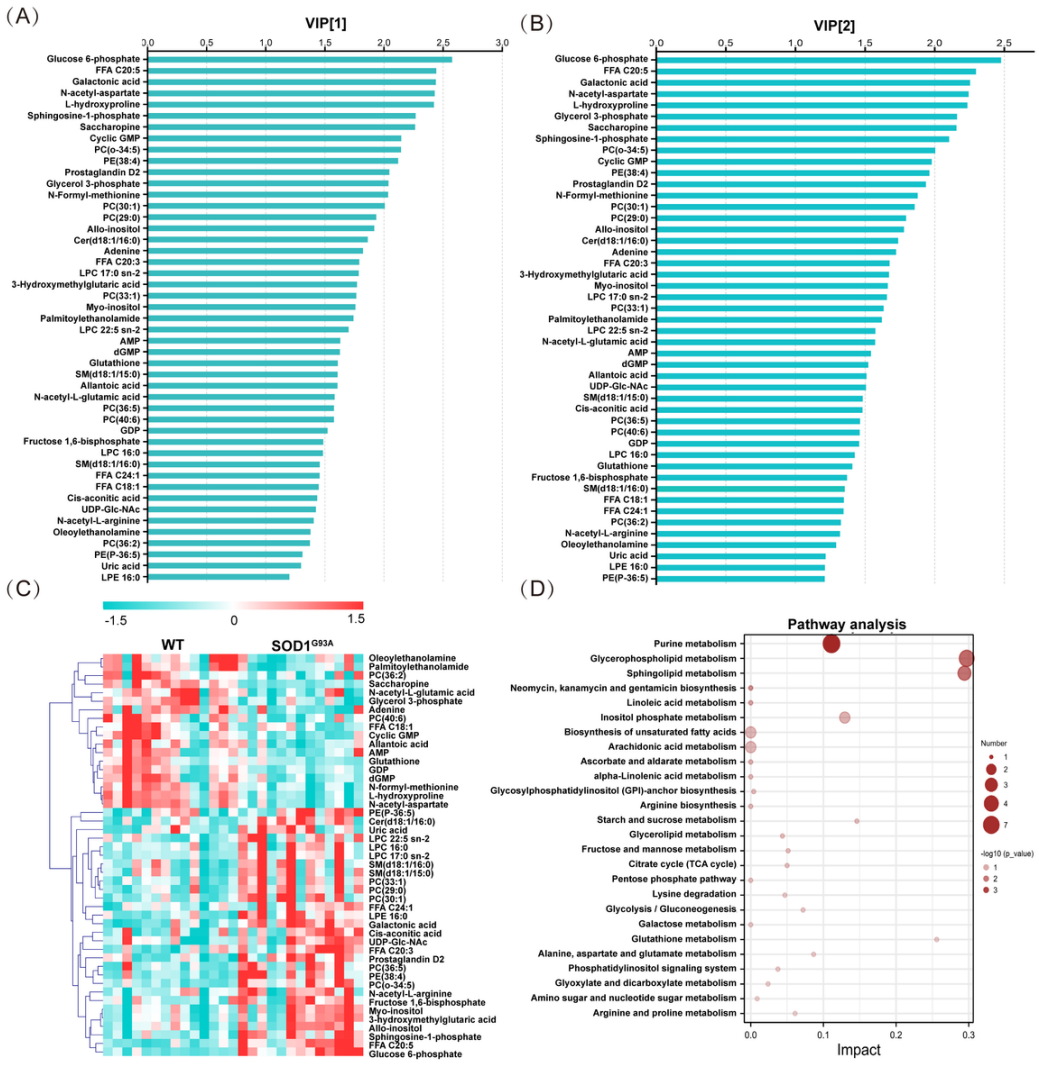


Figure 2

Differential metabolites in spinal cord of SOD1^{G93A}mice in the symptomatic stage. **(A)** VIP [1] score of significant metabolites. **(B)** VIP [2] score of significant metabolites. **(C)** Heat map of the differential metabolites between WT and SOD1G93A mice in the symptomatic stage. (**D**) Pathway analysis of the differential metabolites.

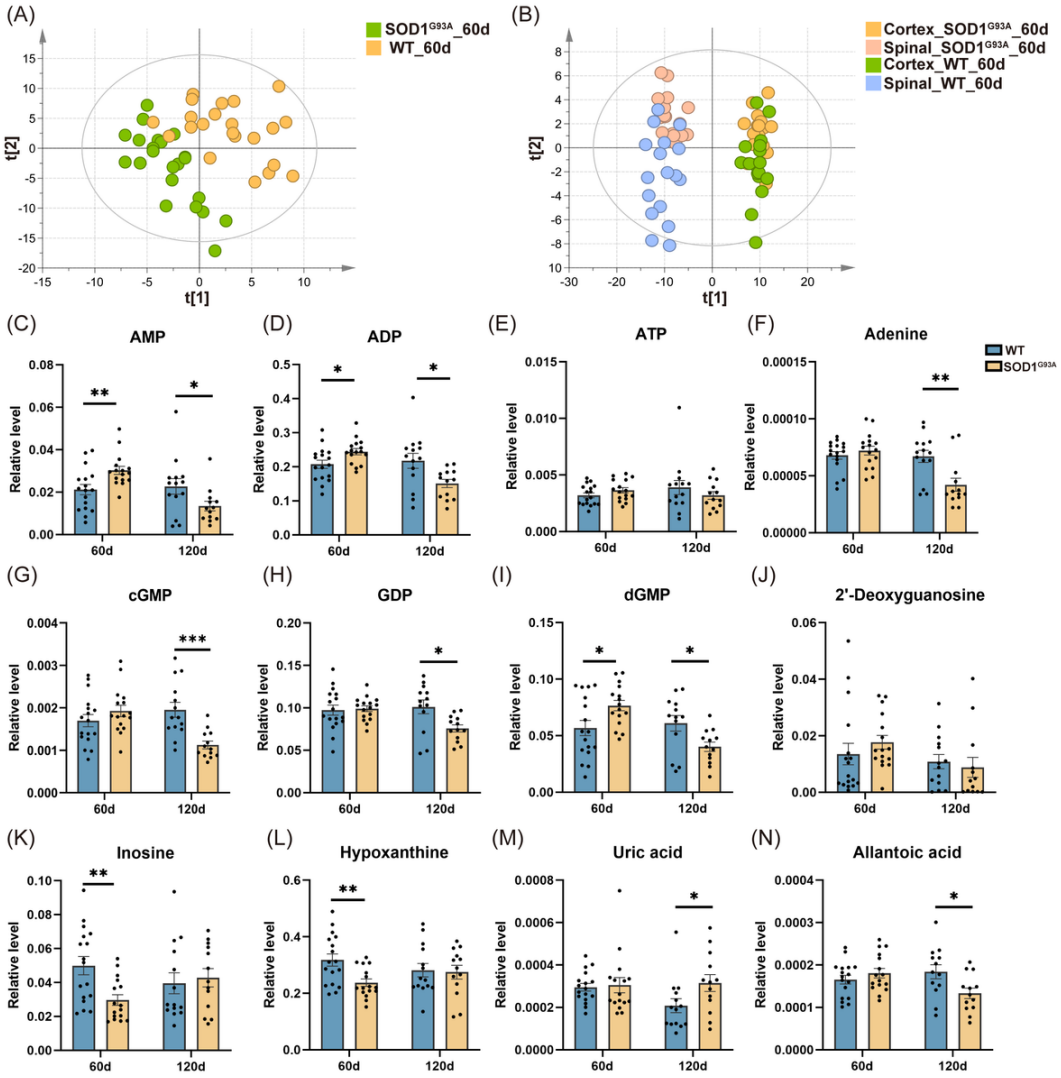


Figure 3

Metabolic disturbances in the pre-symptomatic stage. **(A)** PLS-DA score plot of metabolome in plasma of mice at 60 days of age. Model parameters: R2X = 0.23, R2Y = 0.708, Q2 = 0.304. CV-ANOVA data: $p = 0.01$, F factor = 3.76. **(B)** PLS-DA score plot of metabolome in cortex and spinal cord of mice at 60 days of age. Model parameters: R2X = 0.376, R2Y = 0.451, Q2 = 0.299. CV-ANOVA data: $p = 0$, F factor = 5.6. **(C–N)** Bar graphs of the 12 purine and purine derivative metabolites in the spinal cord of WT and $SOD1^{G93A}$ mice at 60 and 120 days old. The values are expressed as mean ± SEM, * $p < 0.05$ versus age-matched WT mice, ** $p < 0.001$ versus age-matched WT mice, *** $p < 0.001$ versus age-matched WT mice, by multiple unpaired t-test.

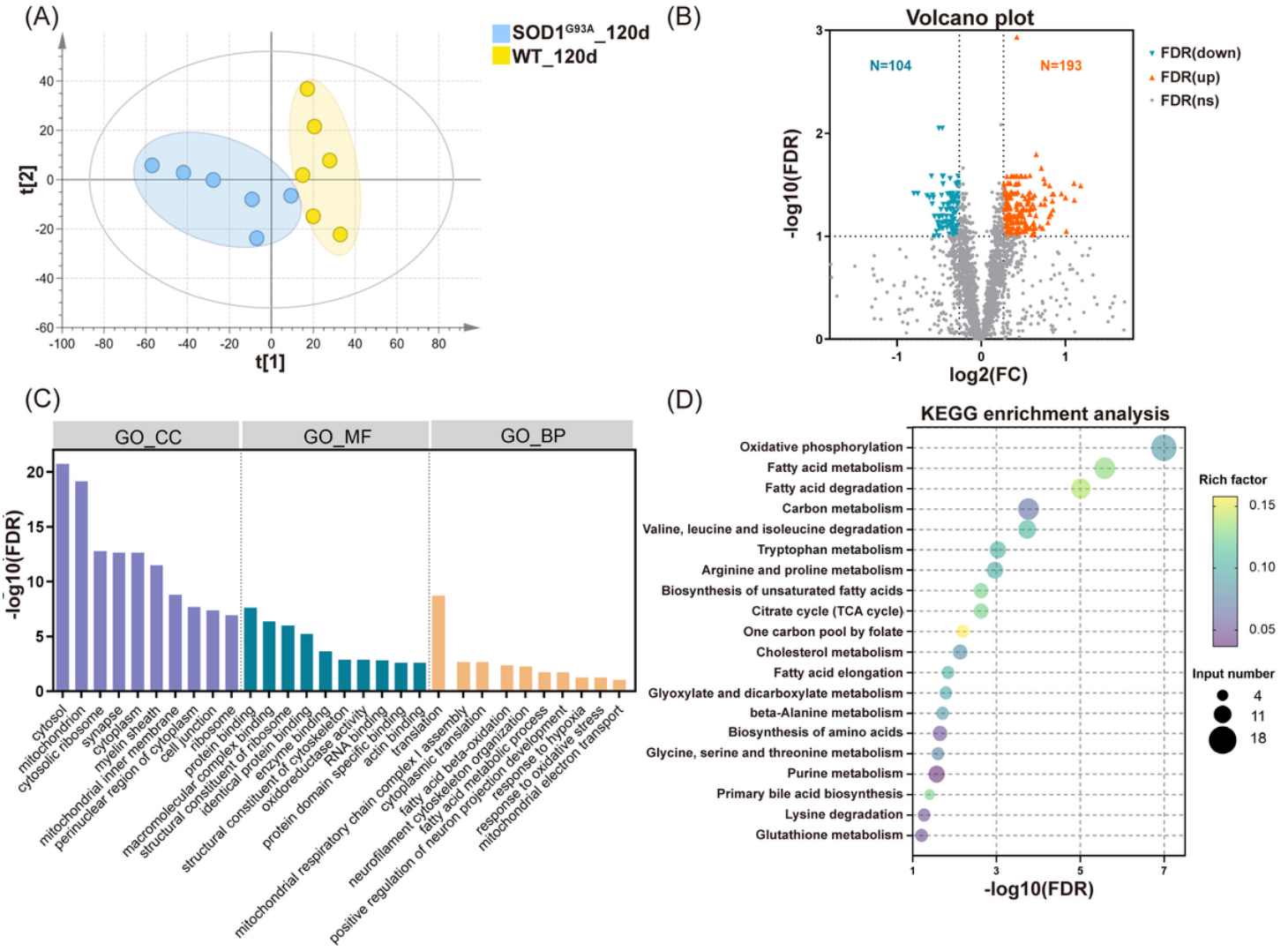


Figure 4

Differentially expressed protein in spinal cord at the symptomatic stage. **(A)** PCA score plot of plasma proteome of mice at 120 days old. **(B)** Volcano plot of differential expressed proteins. **(C)** Top 10 terms of CC, MF, and BP in GO annotation analysis. **(D)** Top 20 terms related to metabolism in the KEGG enrichment analysis.

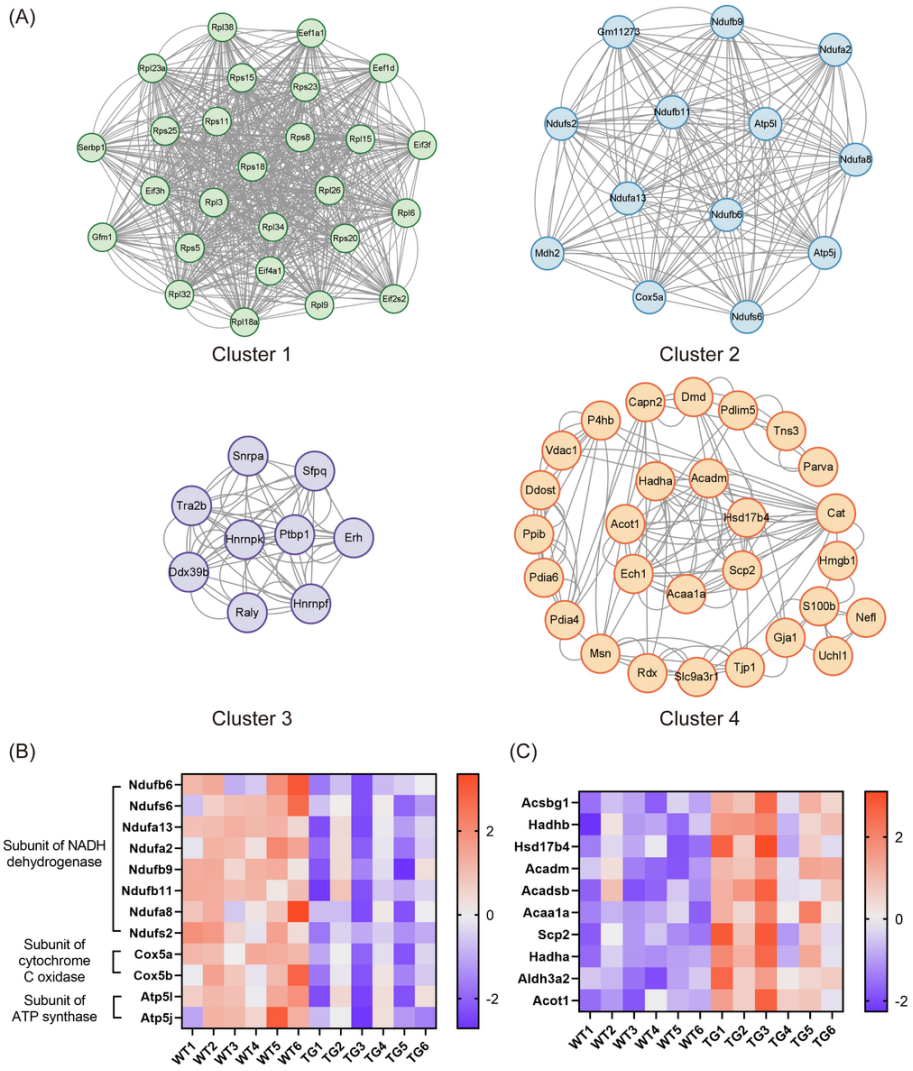


Figure 5

MCODE analysis and DEPs involved in OXOPHS and fatty acid metabolism. **(A)** Proteins and interactions of four significant clusters identified by MCODE analysis. **(B)** Heat map of DEPs involved in OXOPHS. **(C)** Heat map of DEPs involved in fatty acid metabolism.

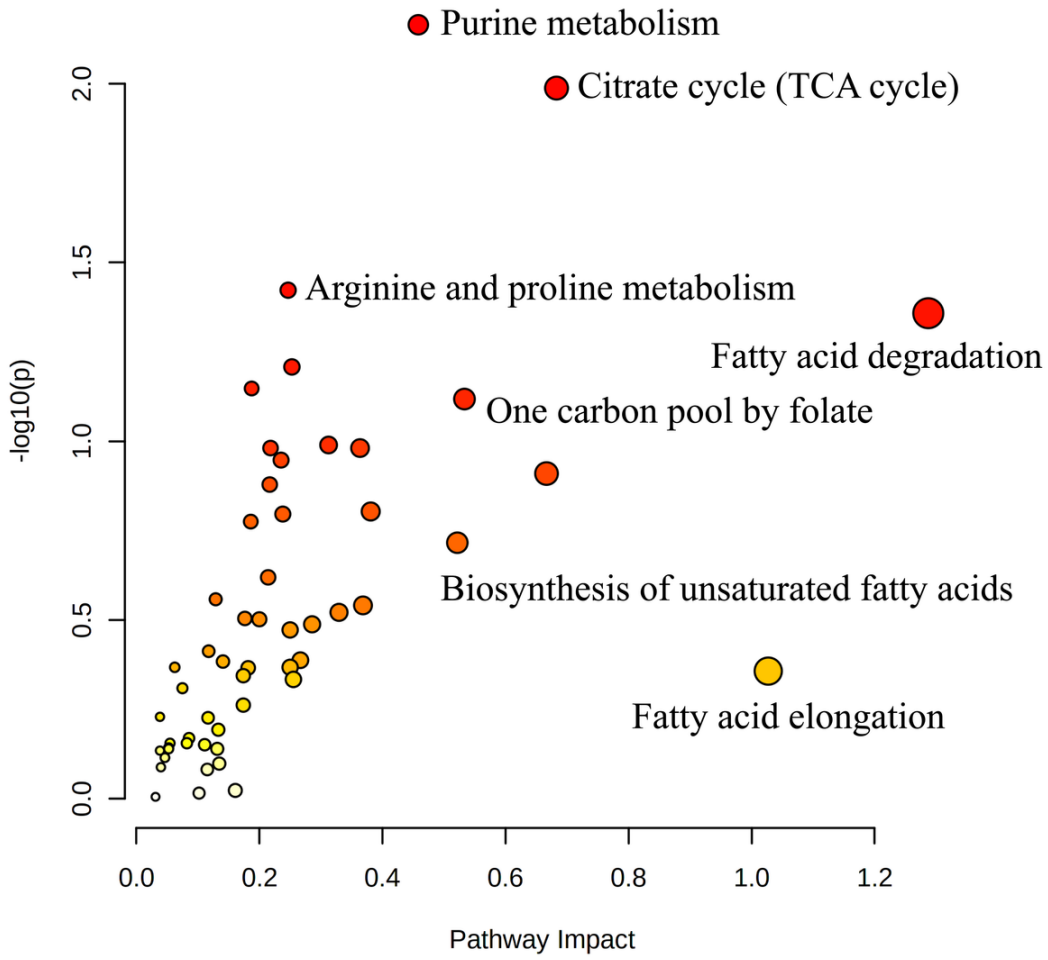


Figure 6

Joint-pathway analysis of proteomics and metabolomics.

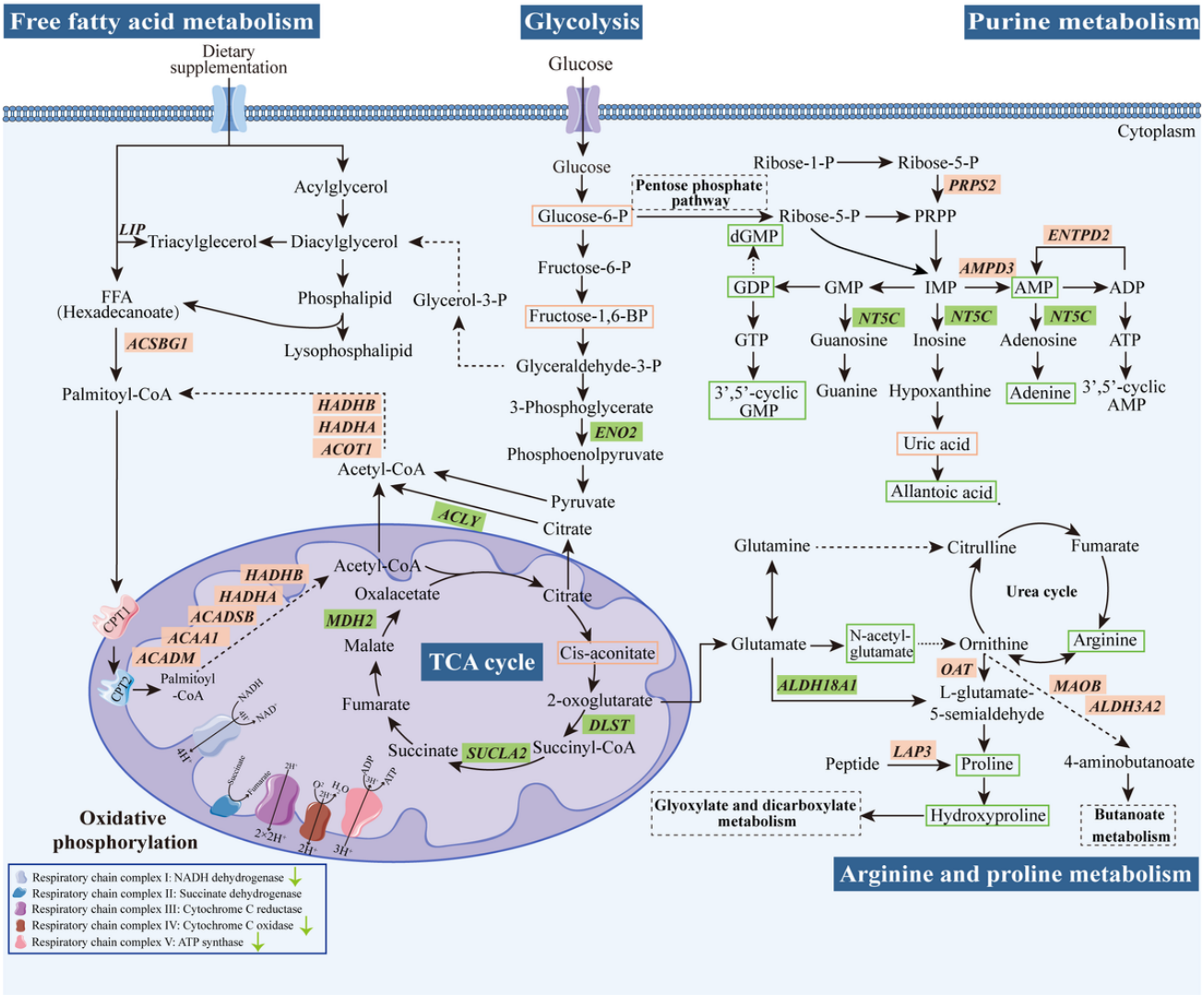


Figure 7

The most perturbed metabolic pathways involved in the SOD1G93A mice model. PRPS2, phosphoribosyl pyrophosphate synthetase 2; ENTPD2, ectonucleoside triphosphate diphosphohydrolase 2; AMPD3, adenosine monophosphate deaminase 3; NT5C, 5', 3'-nucleotidase, cytosolic; ACLY, ATP citrate lyase; DLST, succinyltransferase; SUCLA2, succinate-CoA ligase; MDH2, malate dehydrogenase 2; HADHA, hydroxyacyl-coenzyme A dehydrogenase alpha subunit; HADHB, hydroxyacyl-coenzyme A dehydrogenase beta subunit; ACADM, acyl-CoA dehydrogenase medium chain; ACAA1, acetyl-CoA acyltransferase 1, ACADSB, acyl-coenzyme A dehydrogenase, short/branched chain; ACOT1, acyl-CoA thioesterase 1; Eno2, enolase 2, gamma neuronal; Aldh18a1, aldehyde dehydrogenase 18 family, member A1; LAP3, leucine aminopeptidase 3; OAT, ornithine aminotransferase; MAOB, monoamine oxidase B; ALDH3A2. aldehyde dehydrogenase family 3, subfamily A2.

Supplementary Files

This is a list of supplementary files associated with this preprint. Click to download.

- Additionalfile1.docx
- Additionalfile2.xlsx